Applied Physics Letters

RESEARCH ARTICLE | FEBRUARY 20 2024

Metasurface-empowered high-efficiency and broadband terahertz vortex beam plates

Li Niu ; Xieyu Chen ; Yuanhao Lang ; Quan Xu ; Xueqian Zhang ; Jiajun Ma; Chunmei Ouyang ; Zhen Tian ; Jiaguang Han ; Weili Zhang

Appl. Phys. Lett. 124, 081701 (2024)
https://doi.org/10.1063/5.0183220

AIP Publishing

Applied Physics Letters ARTICLE pubs.aip.org/aip/apl

Metasurface-empowered high-efficiency and broadband terahertz vortex beam plates

Cite as: Appl. Phys. Lett. **124**, 081701 (2024); doi: 10.1063/5.0183220
Submitted: 21 October 2023 · Accepted: 21 January 2024 ·
Published Online: 20 February 2024

Li Niu,[1] Xieyu Chen,[1,2] Yuanhao Lang,[1] Quan Xu,[1,a)] Xueqian Zhang,[1] Jiajun Ma,[1] Chunmei Ouyang,[1] Zhen Tian,[1,a)] Jiaguang Han,[1,3,a)] and Weili Zhang[4]

AFFILIATIONS

[1]Center for Terahertz Waves and College of Precision Instrument and Optoelectronics Engineering, Tianjin University, Tianjin 300072, China
[2]Research Center for Intelligent Chips and Devices, Zhejiang Lab, Hangzhou 311121, China
[3]Guangxi Key Laboratory of Optoelectronic Information Processing School of Optoelectronic Engineering, Guilin University of Electronic Technology, Guilin 541004, People's Republic of China
[4]School of Electrical and Computer Engineering, Oklahoma State University, Stillwater, Oklahoma 74078, USA

[a)]**Authors to whom correspondence should be addressed:** quanxu@tju.edu.cn; tianzhen@tju.edu.cn; and jiaghan@tju.edu.cn

ABSTRACT

Metasurfaces have been continuously garnering attention in both scientific and industrial fields owing to their unprecedented wavefront manipulation capabilities using arranged subwavelength artificial structures. Terahertz vortex beams have become a focus of research in recent years due to their prominent role in many cutting-edge applications. However, traditional terahertz vortex beam plates are often faced with challenges including large size, low efficiency, and limited working bandwidth. Here, we propose and experimentally demonstrate highly efficient and broadband vortex beam plates based on metasurface in the terahertz region. The experimental results well verify that the designed metasurfaces can efficiently generate terahertz vortex beams with different orbital angular momentum topological charges in the range of 0.5–1 THz. Notably, the maximum efficiency can reach about 65% at 0.5 THz. The proposed devices may play a vital role in developing vortex beams-related terahertz applications.

Terahertz technology has garnered significant attention recently due to its promising applications in spectroscopy,[1,2] imaging,[3] and ultrafast communications.[4–6] In parallel, the emergence of vortex beams, characterized by helical wavefronts and optical orbital angular momentum (OAM), has led to a revolution in the fields of quantum information,[7–9] optical trapping,[10–12] communications,[13–15] etc. Particularly, terahertz vortex beams have attracted widespread attention owing to their distinctive fusion of terahertz waves and OAMs. This combination of unique advantages positions them as highly promising tools in sensing of magnetic excitations,[16] data encoding,[17,18] self-healing,[19] terahertz communications, and imaging.[20] They facilitate OAM multiplexing, thereby enhancing the efficiency of data transmission.[21,22] Furthermore, in the realm of imaging, they provide a way to break through the limit and help achieve super-resolution imaging.[23] Consequently, there is a substantial demand for terahertz vortex beams, driving an urgent need for the efficient and wideband generation of these beams. However, traditional vortex beam plates often encounter the challenge of achieving both high efficiency and broadband performance simultaneously, which hinders the widespread application of terahertz vortex beams.[24,25]

Potential viable solutions for achieving broadband terahertz vortex beams include multilayer achromatic wave plates, total internal reflection devices, liquid crystal-based devices, and metasurfaces.[26] Among these, metasurfaces stand out as an exotic and appealing platform for the design of functional devices, making them the primary candidate for future broadband THz beam shapers.[27–29] By arranging artificial microstructures at sub-wavelength scale according to a certain spatial order, the metasurface can achieve various devices, including beam deflectors,[30–32] metalenses,[33–35] special beam generators,[36–38] and meta-holograms.[39,40] In particular, different terahertz vortex beam plates have been demonstrated by single-layer transmission metasurfaces,[41,42] reflection metasurfaces,[43] and all-dielectric metasurfaces.[44–48] Despite this progress, reflection metasurfaces promise increased efficiency but require complex optical configurations for integration;[43] single-layer transmission metasurfaces[41,42] and all-dielectric metasurfaces both face an upper limit on achievable efficiency.[44–48] Multilayer

metasurfaces employ Fabry–Pérot cavities for efficient polarization conversion and phase control, ensuring broadband performance and augmenting wavefront control efficiency.[49,50] This development offers a promising pathway for the advancement of efficient and wideband multifunctional wavefront manipulation techniques, potentially impacting various domains within the realms of science and technology.

In this Letter, we propose and experimentally demonstrated highly efficient and broadband flexible vortex beam plates functioning at terahertz frequencies. The terahertz vortex beam plates utilize a three-layer structure. The upper and lower layers consist of orthogonal gratings, while the middle layer comprises microstructures of varying sizes. This configuration forms a Fabry–Pérot cavity, enabling efficient broadband polarization conversion, as well as precise phase control, thus facilitating the efficient generation of vortex beams. We designed and fabricated vortex beam plates with topological charge from −5 to +5, which can realize the generation of high efficiency vortex beams in a wide band range from 0.5 to 1 THz, in which the maximum efficiency can reach about 65% at 0.5 THz. Moreover, utilizing flexible organic film polyimide (PI) materials as the dielectric layer enables the device to potentially operate under some deformations. Such devices have a certain tolerance for fabrication alignment and can be very promising in developing next-generation efficient and ultracompact terahertz functional devices.

As illustrated in Fig. 1(a), the designed freestanding terahertz vortex beam plate is a sandwiched device with three aluminum structure layers separated by two polyimide spacers. The central metallic layer consists of square-split-ring (SSR) structures set at a diagonal angle of 45° to maximize the conversion efficiency of linearly polarized light. We can expect that the normally incident y-polarization wave propagating along the z axis direction is converted to the transmitted x-polarization wave passing through the proposed vortex plate. In general, for a single-layer transmissive plasmonic metasurface, the orthogonally polarized light transmission is less than 0.5. To further improve the conversion efficiency, two mutually orthogonal metal grating layers with the same period of 50 μm and duty cycle of 50% are designed on both sides of the SSR layer. Such a tri-layered structure can form a Fabry–Pérot resonance cavity, which could allow multiple electromagnetic wave reflection and transmission, thus resulting in enhancing the polarization conversion efficiency and extending the operation bandwidth. By carefully adjusting the thickness of PI spaces, the transmission amplitude of orthogonally polarized light can reach nearly 1 in a broadband range according to the Fabry–Pérot resonance effect[50] (for more details, see Sec. S1 of the supplementary material).

To realize the generation of terahertz vortex beam, it is crucial to achieve a group of unit cells that enable abrupt phase shift covering a 360° range and a nearly constant transmission amplitude simultaneously. In our design, this requirement can be satisfied by carefully tailoring the geometrical parameter g and thus the gap size of SSR. First, we investigate the cross-polarized component transmission of unit cell structures under different values of g using a commercial full-wave numerical software computer simulation technology (CST) Microwave Studio. According to the simulation results, four unit cells (from #1 to #4) with different gap sizes of SSR, which can evenly cover the 180° phase range, are obtained, as shown in Fig. 1(d). By mirroring the unit cell structure from #1 to #4, we create four new structures, labeled as #5, #6, #7, and #8. These structures exhibit cross-polarized radiation with an additional 180° phase shift. This is apparent when observing that the currents leading to cross-polarized radiation are out of phase[51] (see Sec. S2 of the supplementary material). The amplitude and phase of cross-polarized light for unit cell structures from #1 to #8 were obtained through numerical simulations. These results are illustrated in Figs. 1(c) and 1(d), respectively. It can be seen that from 0.5 to 1 THz, the orthogonal polarization mode transmission varies between 0.8 and 0.91 for all unit cells, which is much higher than a single-layer plasmonic metasurface. Moreover, the transmission phase of all unit cells can approximately remain constant within such a frequency regime. The above simulation results indicate that we can use such eight-level phase modulation unit cells to design broadband transmissive terahertz functional devices with relatively high transmission efficiency.

By arranging the eight unit cells according to the phase distribution requirement, several devices, which can generate terahertz vortex beams with different topological charges, are designed. To further investigate the performance of such vortex beam plates, the devices were fabricated using a multilayer photolithography process. First, a

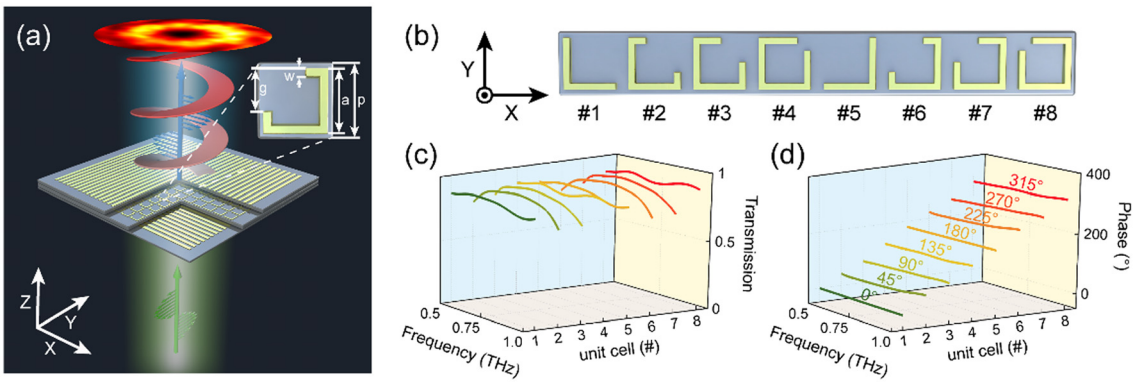

FIG. 1. Schematic view of the THz vortex beam plate and eight-level phase modulation unit cell design. (a) Schematic diagram of the terahertz vortex beam plate and the unit cell of the middle metallic layer. (b) Selected unit cells for eight-level phase modulation with fixed parameters, p = 100 μm, a = 80 μm, and w = 10 μm. The parameter g of unit cells from #1 to #4 are 70, 52.5, 37.5, and 20 μm, respectively. The unit cells from #5 to #8 are obtained by a rotating structure, from #1 to #4 by 90° counterclockwise. (c) and (d) Simulated transmission and phase spectra of eight complete unit cells from 0.5 to 1 THz, respectively.

10 μm thick PI layer was spin-coated onto a polished silicon substrate with a thickness of 1 mm to protect the bottom metal layer. Then, the bottom grating layer of 200 nm thick aluminum was thermally evaporated following standard photolithography process. Next, another PI layer of 25 μm thickness was spin-coated on the grating layer. It should be noted that for such a thick PI layer, the spin-coating process needs to be repeated several times. The next metal and PI layers were fabricated by repeating the above-mentioned process. Finally, the sample was peeled off from the silicon substrate and mounted on a prepared holder, as illustrated in Fig. 2(a). An optical microscope image of one of the vortex beam plate samples is shown in Fig. 2(b). However, due to the shield of metallic grating structure, only the first grating layer can be seen in the photography. To distinctly illustrate the difference in the unit cell arrangement among different sample elements, we provide microscopy images of the central region of the vortex beam sample with topological charges ranging from +1 to +5, along with a schematic diagram depicting the arrangement of unit cells (see Sec. S3 of the supplementary material). It is also worth noting that our design has a certain tolerance for fabrication accuracy, because the upper and lower structures are equivalent to a set of orthogonal placement of the grating, and the middle layer of the structure is set to achieve polarization conversion and phase control. The function of each layer is relatively independent, so when there is a certain error in sample alignment, it will not have a relatively large impact on the final result (for more details, see Sec. S4 of the supplementary material). Additionally, due to the flexible polyimide (PI) dielectric layer used in the sample, it exhibits a notable capacity for bending (see Sec. S5 of the supplementary material). It offers tuning advantages through mechanical deformation, and the prospect of integrating devices with flexible substrates holds promise for collaboration with other components and non-planar structures.[52]

Next, the fabricated vortex beam plates were characterized using a fiber-based terahertz time-domain scanning microscopy[53] (for more details, see Sec. S6 of the supplementary material) with a broadband width (0.2–1.2 THz), as illustrated in Fig. 2(c). The *x*-polarized terahertz beam was generated from a photoconductive antenna-based emitter and collimated by a lens to form a quasi-Gauss beam. The detector was a near-field photoconductive-antenna-based probe that could measure the THz field by a pair of electrodes sensitive to the *Ex* component. We integrated a terahertz grid polarizer with a 45° orientation angle between the lens and the sample to enable a broadband *y*-polarized component incidence on the sample. It is worth noting that the use of broadband achromatic wave plates here can achieve more efficient polarization conversion.[54,55] The bottom grating of the sample is equivalent to the polarizer and will block the remaining *x*-polarized component, so it will not affect the experimental results. Our metasurface performs orthogonal polarization conversion. After modulation by prepared samples, the electric field distribution of the generated *x*-polarized terahertz vortex beams with different topological charges was recorded by the mechanically scanning terahertz probe.

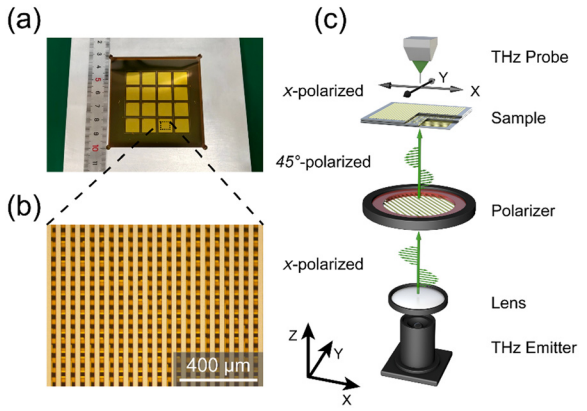

FIG. 2. Fabricated samples and experimental setup. (a) A photograph of a mounted terahertz vortex beam plate sample. (b) Optical microscope image of one of the vortex beam plate devices. (c) Schematic view of the experimental setup.

The measured results of generated terahertz vortex beams carrying different orbital angular momentum at 0.75 THz are summarized in Fig. 3. As expected, hollow intensity distribution caused by the phase singularity can be clearly seen for all vortex beams, as illustrated in Figs. 3(a) and 3(d). The central dark area of the vortices gradually enlarges with increased topological charge. Additionally, it can be seen that the concentric intensity distribution along the radial direction accords with the characteristics of Kummer function, known as the Kummer beam.[56] The formation of the Kummer beam results from the diffraction of a Gaussian beam at the on-axis singular point, which becomes apparent in the field after its propagation through the metasurface. Furthermore, in the intensity distribution diagrams of Figs. 3(a) and 3(d), eight symmetrical lobes surround the vortex beam, with the +1 and −1 orders being particularly pronounced. This phenomenon results from selecting eight element structures with a distinct phase difference of $\pi/4$, as illustrated in Fig. S3(a), to construct the vortex beam plate. The discrete phase distribution introduces additional field disturbances due to phase jumps at radial junctions.[56] Moreover, as shown in Figs. 3(b) and 3(e), the azimuthal angle dependence phase distribution with a phase singularity at the center can also be seen, which reveals the vortex nature of the generated terahertz beams. To quantitatively evaluate the quality of terahertz vortex beams, we calculate the purity of the vortex beam. Since the angular harmonics, $\exp(il\varphi)$, are orthogonal over the azimuthal plane, we assume the complex amplitude of superposition field of a terahertz beam in terms of harmonics in a plane perpendicular to the optical axis z to be given by[57,58]

$$E_f(r,\theta,z) = \frac{1}{\sqrt{2\pi}} \sum_l S_{f,l}(r,z) \exp(il\theta) \tag{1}$$

with

$$S_{f,l}(r,z) = \frac{1}{\sqrt{2\pi}} \int_{-\pi}^{\pi} E_f(r,\theta,z) \exp(-il\theta) d\theta, \tag{2}$$

where $E_f(r,\theta,z)$ is the complex electric field along closed loops enclosing the beam center at different radii and frequency f. To quantitatively evaluate the quality of terahertz vortex beams, six rings were selected to calculate the purity. The radii were chosen in the form $m\Delta r$ (m = 1, …, 6), ensuring that 80% of the incident beam energy was contained within a radius of $6\Delta r$, $\int_0^{6\Delta r} |E_f(r,\theta,z)|^2 r dr d\theta = 0.8 \int_0^{\infty} |E_f(r,\theta,z)|^2 r dr d\theta$.[57] According to measured terahertz vortex beams with different topological charges at 0.75 THz, the radius we selected is shown in white dotted circles on the intensity profiles of Figs. 3(a) and 3(d). By substituting the electric field along the different radius into Eq. (2), the calculated OAM spectrum coefficients $|S_{f,l}|^2$ normalized by the maximum value are

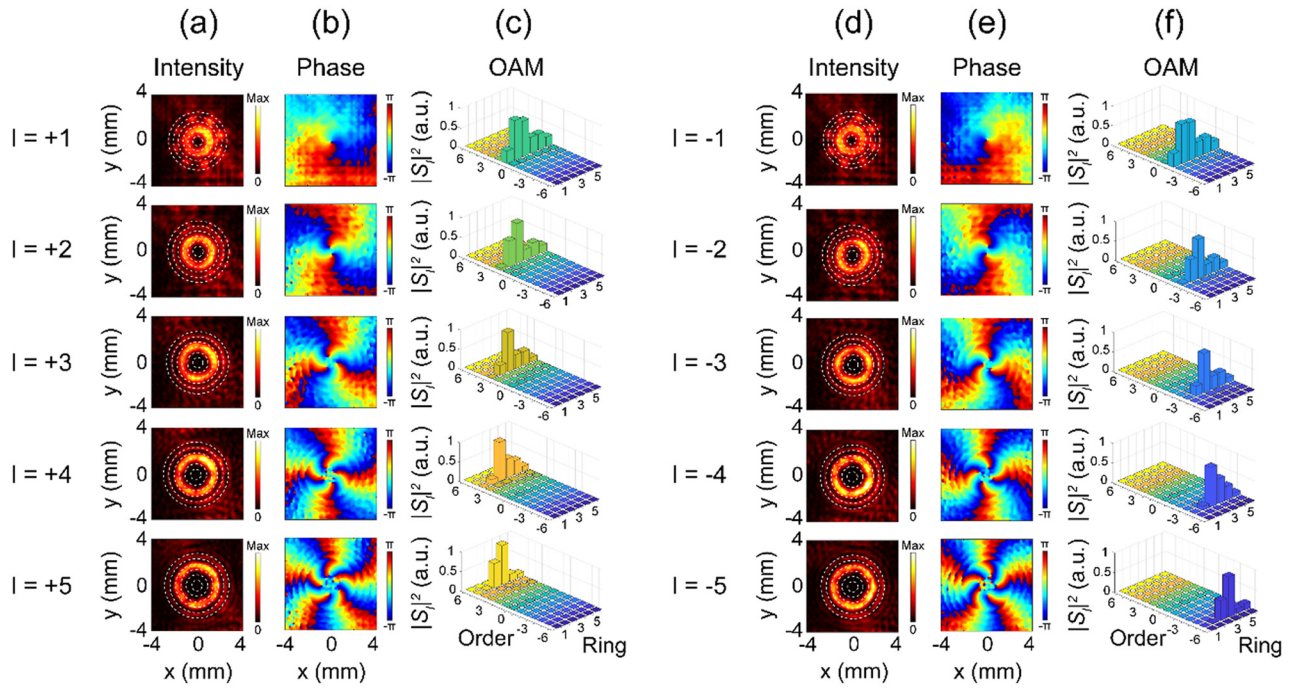

FIG. 3. (a)–(f) Measured terahertz vortex beams with different topological charges at 0.75 THz. (a)–(c) Measured intensity distributions, phase distributions, and OAM spectrum $|S_{0.75\mathrm{THz},\,l}|^2$ of terahertz vortex beams with topological charge l changing from $+1$ to $+5$, respectively. (d)–(f) Measured intensity distributions, phase distributions, and OAM spectrum $|S_{0.75\mathrm{THz},\,l}|^2$ of terahertz vortex beams with topological charge l changing from -1 to -5, respectively. The measured OAM spectrum (for l values of -5 to $+5$) as a function of the radial ring on the beam. The white dotted circle shown on the intensity profiles are integrated loops used to extract the OAM complex amplitude of different vortex beams. The height of each bar represents the measured coefficients $|S_{0.75\mathrm{THz},\,l}|^2$.

depicted in Figs. 3(c) and 3(f). Despite variations in the strength of the electric field across different radius rings, it is evident that the dominant OAM component order of each vortex beam aligns with our design. Simultaneously, the presence of other OAM components is observed to be relatively weak, indicating high mode purity of generated terahertz vortex beams. These experimental results clearly show the ability to generate terahertz vortex beams carrying different OAM of the proposed devices.

To further verify the broadband performance, the quality of the generated vortex beam with topological charge of $+3$ under different frequencies from 0.5 to 1 THz is also evaluated. The time-domain signals at different points are acquired through point-by-point scanning of the terahertz near-field probe. Subsequently, the electric field distributions at different frequencies can be obtained through Fourier transform, as illustrated in Fig. 4. In Fig. 4(a), an annular intensity distribution with a null area at the center is depicted, while Fig. 4(b) illustrates a helical phase distribution undergoing three cycles from $-\pi$ to π. This observation is consistent across the frequency range from 0.5 THz to 1 THz, indicating the third-order vortex nature of the generated terahertz beam. The vortex beams generated at different frequencies appear generally uniform, with only a small amount of stray light observed at 0.9 and 1.0 THz. This can be attributed to the distribution of the incident beam spots at the corresponding frequencies (see Secs. S7 and S8 of the supplementary material). The OAM coefficients $|S_{f,l}|^2$ of vortex beams corresponding to different frequencies are also extracted and shown in Fig. 4(c). It can be found that the third-order OAM component is the strongest, while the other orders are quite weak, indicating the high purity of generated third-order vortex beams for all frequencies. The measured results clearly show that the proposed device can generate high quality terahertz vortex beams in a broadband regime ranging from 0.5 to 1 THz.

To better use vortex light in terahertz communication, imaging, and other fields, it is essential to achieve efficient and broadband terahertz vortex generation. To characterize the efficiency of the terahertz vortex beam plate, we first measured the terahertz spot without the sample using near-field terahertz imaging system, and then the electric field distribution of the vortex beam with different topological charges generated after passing through the sample was measured. The efficiency of terahertz vortex beam plate can be calculated by $\eta = P_s/P_r$, where P_s and P_r represent the integrated results of the intensity distributions of the vortex beams that pass through the sample and the incident spot, respectively. Based on such a definition, the efficiency of vortex beams with different topological charges at different frequencies was calculated using the experimental results, as shown in Fig. 5. To more precisely depict the performance of the vortex beam plate, we present the variation in generation efficiency of the vortex beam across different topological charges and frequencies (see Sec. S9 of the supplementary material). We can see that all of the vortex beams with topological charge from -5 to $+5$ maintain relatively high efficiency in the broadband range from 0.5 to 1 THz. As the frequency decreases, the efficiency will gradually increase. The vortex generation efficiency for different topological charges in the range of 0.5–1 THz consistently

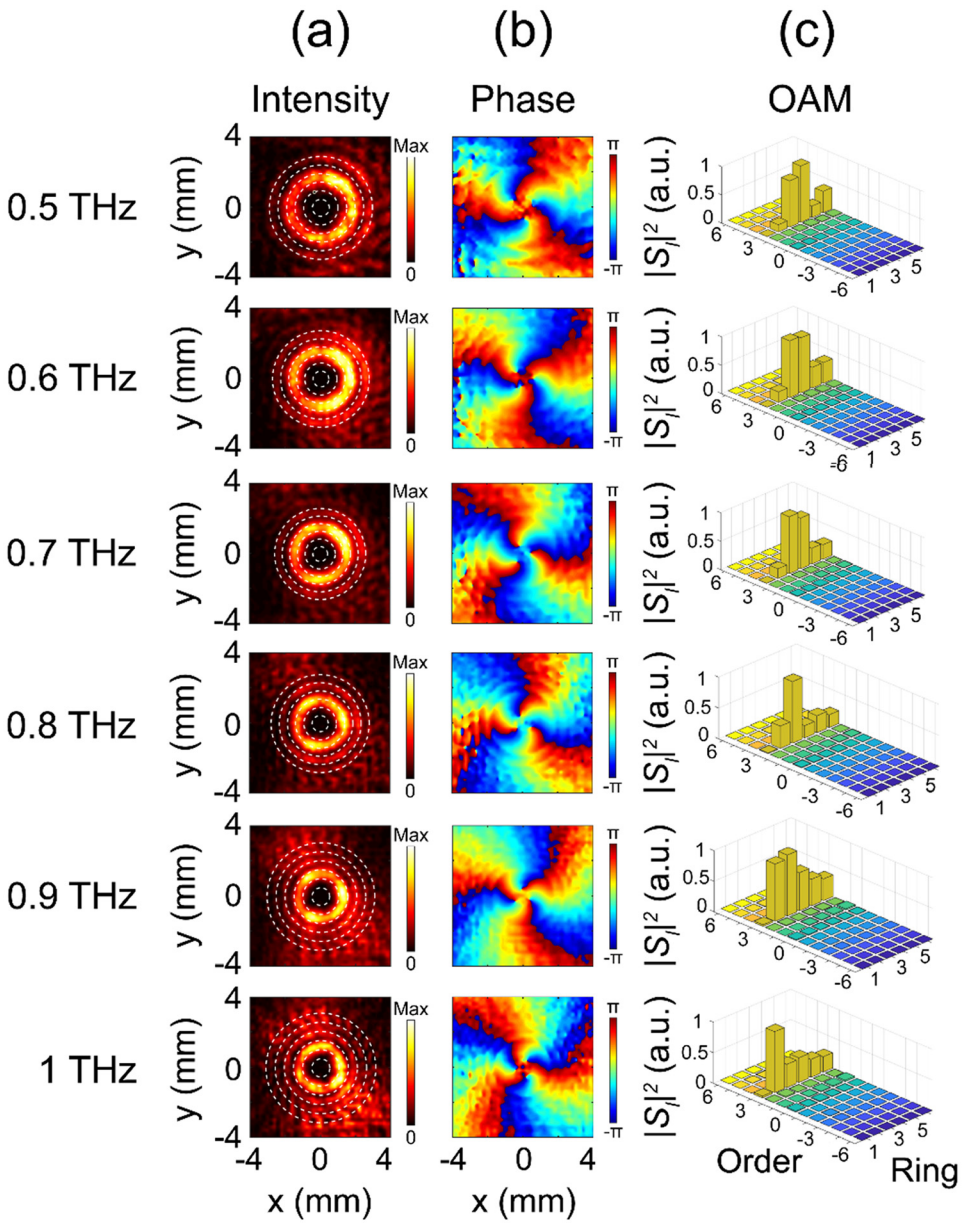

FIG. 4. Measured THz vortex beams with topological charge $l = +3$ under different frequencies. (a)–(c) Measured intensity distributions, phase distributions, and OAM spectrum $|S_{f,\,l}|^2$ of terahertz vortex beams with topological charge $l = +3$ under different frequencies of 0.5, 0.6, 0.7, 0.8, 0.9, and 1 THz, respectively. The white dotted circles shown on the intensity profiles are integrated loops used to extract the OAM complex amplitude of different vortex beams. The height of each bar represents the measured coefficients $|S_{f,\,l}|^2$.

exceeds 37%, with a peak efficiency observed at 0.5 THz, reaching approximately 65%. We compare these values with other terahertz vortex beam plates including Q plate, spiral phase plate, plasmonic metasurface, and dielectric metasurface and summarize the results in Table I. All the data presented in the table represents experimental results. Compared with the currently prevalent terahertz vortex beam generators outlined in Table I, there are a few methods that can simultaneously achieve both the bandwidth and efficiency demonstrated in our approach. Traditional terahertz vortex plates, such as the Q plate and the spiral phase plate, demonstrate relatively high efficiency but are tailored to specific frequencies. While the specific vortex beam generation efficiency is not provided for single-layer plasmonic metasurfaces, the efficiency of vortex beam generation is constrained by a maximum cross-polarization conversion efficiency of 25%.[59,60] The dielectric metasurface is also unable to simultaneously surpass the bandwidth and efficiency of this design. By comparing these results, it becomes increasingly evident that our design can indeed attain both high efficiency and broad-ranging advantages. Moreover, the performance of the device can be further improved by selecting a structure with high amplitude and 2π phase coverage in the wideband range. If a reflective design could be adopted, it could achieve even broader vortex generation.[61] This work lays a solid foundation for its future applications in the terahertz field.

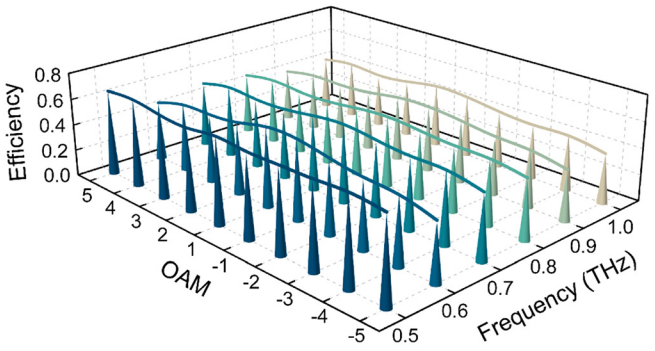

FIG. 5. Measured generation efficiency under different frequencies and topological charges of designed terahertz vortex beam plates.

TABLE I. Comparison of terahertz vortex beam plates.

Generating OAM schemes	Working efficiency	Working frequency (THz)
Q plate	50%	1 (Ref. 24)
Spiral phase plate	90%	2 (Ref. 25)
Plasmonic metasurface	NA	0.75 (Ref. 41)
	NA	0.5–0.9 (Ref. 42)
Dielectric metasurface	60%	1.1 (Ref. 44)
	57.8%	0.6 (Ref. 45)
	55.1%	1.0 (Ref. 46)
	75.2%	1.0 (Ref. 47)
	25%	0.75–0.9 (Ref. 48)
This work	65%–37%	0.5–1.0

In conclusion, we propose transmission-type terahertz vortex plates based on a multilayer metasurface, which are experimentally proven to have wideband and high efficiency. Adopting the multilayer structure to achieve the efficient broadband manipulation of the orthogonally polarized terahertz wave, we experimentally illustrate that the proposed design scheme has superior performance in generating terahertz vortex beam. The experiments demonstrated that all of the vortex beams with topological charge from −5 to +5 maintain relatively high efficiency in the broadband range from 0.5 to 1 THz, where the maximum efficiency can reach about 65% at 0.5 THz. In addition, the performance of generating vortex beams is robust due to the high tolerance of alignment accuracy during fabrication. The findings from this work would open an avenue toward the application of vortex beams in terahertz communications. We envision that our work may boost further endeavors into the design and fabrication of different terahertz devices, making them very promising in developing next-generation efficient and ultracompact terahertz functional devices.

See the supplementary material for (1) simulation of amplitude and phase of different dielectric layer thicknesses, (2) simulated surface current distribution for unit cells, (3) microscopy images and layout diagram of the sample, (4) simulation on high tolerance of alignment accuracy of samples, (5) photograph of the flexible metasurface sample, (6) experiment setup, (7) measured intensity distributions and phase distribution of the illuminating beam, (8) calculated intensity and phase distribution of the vortex beam at 1 THz, and (9) the measured generation efficiency of the designed terahertz vortex beam plates.

This work was supported by the National Natural Science Foundation of China (Nos. 62375203, 62135008, 62235013, 62075158, and 62025504), the National Science Foundation (No. 2114103), and the Yunnan Expert Workstation (No. 202205AF150008).

AUTHOR DECLARATIONS

Conflict of Interest

The authors have no conflicts to disclose.

Author Contributions

Li Niu, Xieyu Chen, and Yuanhao Lang contributed equally to this work.

Li Niu: Conceptualization (equal); Data curation (equal); Formal analysis (equal); Writing – original draft (lead); Writing – review & editing (supporting). **Xieyu Chen:** Conceptualization (equal); Data curation (equal); Formal analysis (equal); Investigation (equal); Writing – review & editing (equal). **Yuanhao Lang:** Data curation (equal); Formal analysis (equal); Methodology (equal); Validation (equal); Writing – review & editing (equal). **Quan Xu:** Conceptualization (equal); Formal analysis (equal); Funding acquisition (equal); Project administration (equal); Supervision (equal); Writing – review & editing (equal). **Xueqian Zhang:** Formal analysis (equal); Resources (equal); Writing – review & editing (equal). **Jiajun Ma:** Formal analysis (equal); Writing – review & editing (equal). **Chunmei Ouyang:** Writing – review & editing (equal). **Zhen Tian:** Funding acquisition (equal); Project administration (equal); Resources (equal); Supervision (equal); Writing – review & editing (equal). **Jiaguang Han:** Funding acquisition (equal); Project administration (equal); Resources (equal); Supervision (equal); Writing – review & editing (equal). **Weili Zhang:** Funding acquisition (equal); Resources (equal); Supervision (equal); Writing – review & editing (equal).

DATA AVAILABILITY

The data that support the findings of this study are available from the corresponding authors upon reasonable request.

REFERENCES

[1]J. B. Baxter and G. W. Guglietta, Anal. Chem. **83**(12), 4342 (2011).
[2]N. Sirica, R. I. Tobey, L. X. Zhao, G. F. Chen, B. Xu, R. Yang, B. Shen, D. A. Yarotski, P. Bowlan, S. A. Trugman, J. X. Zhu, Y. M. Dai, A. K. Azad, N. Ni, X. G. Qiu, A. J. Taylor, and R. P. Prasankumar, Phys. Rev. Lett. **122**(19), 197401 (2019).
[3]P. U. Jepsen, D. G. Cooke, and M. Koch, Laser Photonics Rev. **5**(1), 124 (2011).
[4]A. Kumar, M. Gupta, P. Pitchappa, N. Wang, P. Szriftgiser, G. Ducournau, and R. Singh, Nat. Commun. **13**(1), 5404 (2022).
[5]T. Nagatsuma, G. Ducournau, and C. C. Renaud, Nat. Photonics **10**(6), 371 (2016).
[6]Y. Yang, Y. Yamagami, X. Yu, P. Pitchappa, J. Webber, B. Zhang, M. Fujita, T. Nagatsuma, and R. Singh, Nat. Photonics **14**(7), 446 (2020).

[7]X. L. Wang, X. D. Cai, Z. E. Su, M. C. Chen, D. Wu, L. Li, N. L. Liu, C. Y. Lu, and J. W. Pan, Nature **518**(7540), 516 (2015).
[8]B. Ndagano, B. Perez-Garcia, F. S. Roux, M. McLaren, C. Rosales-Guzman, Y. Zhang, O. Mouane, R. I. Hernandez-Aranda, T. Konrad, and A. Forbes, Nat. Phys. **13**(4), 397 (2017).
[9]Z. Q. Zhou, Y. L. Hua, X. Liu, G. Chen, J. S. Xu, Y. J. Han, C. F. Li, and G. C. Guo, Phys. Rev. Lett. **115**(7), 070502 (2015).
[10]Y. Zhang, J. Shen, C. Min, Y. Jin, Y. Jiang, J. Liu, S. Zhu, Y. Sheng, A. V. Zayats, and X. Yuan, Nano Lett. **18**(9), 5538 (2018).
[11]M. Padgett and R. Bowman, Nat. Photonics **5**(6), 343 (2011).
[12]L. Gong, B. Gu, G. Rui, Y. Cui, Z. Zhu, and Q. Zhan, Photonics Res. **6**(2), 138 (2018).
[13]Y. Shen, X. Wang, Z. Xie, C. Min, X. Fu, Q. Liu, M. Gong, and X. Yuan, Light: Sci. Appl. **8**, 90 (2019).
[14]Z. Wang, N. Zhang, and X. Yuan, Opt. Express **19**(2), 482 (2011).
[15]M. P. J. Lavery, C. Peuntinger, K. Gunthner, P. Banzer, D. Elser, R. W. Boyd, M. J. Padgett, C. Marquardt, and G. Leuchs, Sci. Adv. **3**(10), e1700552 (2017).
[16]A. A. Sirenko, P. Marsik, C. Bernhard, T. N. Stanislavchuk, V. Kiryukhin, and S. W. Cheong, Phys. Rev. Lett. **122**(23), 237401 (2019).
[17]E. G. Tsiplakova, M. S. Kulya, B. V. Sokolenko, A. A. Gorodetsky, and N. V. Petrov, in 46th International Conference on Infrared, Millimeter and Terahertz Waves (IRMMW-THz), Chengdu, China, 2021.
[18]M. S. Kulya, B. Sokolenko, A. A. Gorodetsky, and N. V. Petrov, Proc. SPIE **11307**, 113070J (2020).
[19]M. Kulya, V. Semenova, A. Gorodetsky, V. G. Bespalov, and N. V. Petrov, Appl. Opt. **58**(5), A90 (2019).
[20]H. Wang, Q. Song, Y. Cai, Q. Lin, X. Lu, H. Shangguan, Y. Ai, and S. Xu, Chin. Phys. B **29**(9), 097404 (2020).
[21]H. Zhao, B. Quan, X. Wang, C. Gu, J. Li, and Y. Zhang, ACS Photonics **5**(5), 1726 (2017).
[22]A. E. Willner, X. Su, H. Zhou, A. Minoofar, Z. Zhao, R. Zhang, M. Tur, A. F. Molisch, D. Lee, and A. Almaiman, J. Opt. **24**(12), 124002 (2022).
[23]K. Miyamoto, B. J. Kang, W. T. Kim, Y. Sasaki, H. Niinomi, K. Suizu, F. Rotermund, and T. Omatsu, Sci. Rep. **6**, 38880 (2016).
[24]S. Ge, P. Chen, Z. Shen, W. Sun, X. Wang, W. Hu, Y. Zhang, and Y. Lu, Opt. Express **25**(11), 12349 (2017).
[25]K. Miyamoto, K. Suizu, T. Akiba, and T. Omatsu, Appl. Phys. Lett. **104**(26), 261104 (2014).
[26]N. V. Petrov, B. Sokolenko, M. S. Kulya, A. Gorodetsky, and A. V. Chernykh, Light: Adv. Manuf. **3**(4), 43 (2022).
[27]Z. Liu, D. Wang, H. Gao, M. Li, H. Zhou, and C. Zhang, Adv. Photonics **5**(3), 034001 (2023).
[28]Q. Xu, Y. Lang, X. Jiang, X. Yuan, Y. Xu, J. Gu, Z. Tian, C. Ouyang, X. Zhang, J. Han, and W. Zhang, Photonics Insights **2**(1), R02 (2023).
[29]A. H. Dorrah and F. Capasso, Science **376**(6591), eabi6860 (2022).
[30]L. Niu, Q. Xu, X. Zhang, Z. Zhang, S. Li, X. Chen, Y. Xu, J. Ma, M. Kang, J. Han, and W. Zhang, ACS Appl. Mater. Interfaces **13**(4), 5844 (2021).
[31]X. Cai, R. Tang, H. Zhou, Q. Li, S. Ma, D. Wang, T. Liu, X. Ling, W. Tan, Q. He, S. Xiao, and L. Zhou, Adv. Photonics **3**(3), 036003 (2021).
[32]A. E. Cardin, S. R. Silva, S. R. Vardeny, W. J. Padilla, A. Saxena, A. J. Taylor, W. J. M. Kort-Kamp, H. T. Chen, D. A. R. Dalvit, and A. K. Azad, Nat. Commun. **11**(1), 1469 (2020).
[33]Y. Xu, J. Gu, Y. Gao, Q. Yang, W. Liu, Z. Yao, Q. Xu, J. Han, and W. Zhang, Adv. Funct. Mater. **33**(35), 2302821 (2023).
[34]B. Yao, X. Zang, Y. Zhu, D. Yu, J. Xie, L. Chen, S. Han, Y. Zhu, and S. Zhuang, Photonics Res. **9**(6), 1019 (2021).
[35]Y. Li, S. Chen, H. Liang, X. Ren, L. Luo, Y. Ling, S. Liu, Y. Su, and S. Wu, PhotoniX **3**(1), 29 (2022).
[36]B. Sun, X. Zang, B. Lu, H. Chi, Y. Zhou, Y. Zhu, and S. Zhuang, Adv. Opt. Mater. **11**, 2301048 (2023).
[37]T. Wu, X. Zhang, Q. Xu, E. Plum, K. Chen, Y. Xu, Y. Lu, H. Zhang, Z. Zhang, X. Chen, G. Ren, L. Niu, Z. Tian, J. Han, and W. Zhang, Adv. Opt. Mater. **10**(1), 2101223 (2021).
[38]H. Sroor, Y. Huang, B. Sephton, D. Naidoo, A. Vallés, V. Ginis, C. Qiu, A. Ambrosio, F. Capasso, and A. Forbes, Nat. Photonics **14**(8), 498 (2020).
[39]T. Wu, Q. Xu, X. Zhang, Y. Xu, X. Chen, X. Feng, L. Niu, F. Huang, J. Han, and W. Zhang, Adv. Sci. **9**(35), 2204664 (2022).
[40]H. Wang, Z. Qin, L. Huang, Y. Li, R. Zhao, H. Zhou, H. He, J. Zhang, and S. Qu, PhotoniX **3**(1), 10 (2022).
[41]J. He, X. Wang, D. Hu, J. Ye, S. Feng, Q. Kan, and Y. Zhang, Opt. Express **21**(17), 20230 (2013).
[42]Y. Tan, K. Qu, K. Chen, J. Wu, L. Feng, S. Yang, B. Chen, Y. Wang, C. Zhang, K. Fan, C. Zhang, J. Zhao, T. Jiang, Y. Feng, and B. Jin, Adv. Opt. Mater. **10**(16), 2200565 (2022).
[43]J. S. Li and L. N. Zhang, Opt. Express **28**(24), 36403 (2020).
[44]Y. Xu, H. Zhang, Q. Li, X. Zhang, Q. Xu, W. Zhang, C. Hu, X. Zhang, J. Han, and W. Zhang, Nanophotonics **9**(10), 3393 (2020).
[45]F. Huang, Q. Xu, W. Liu, T. Wu, J. Gu, J. Han, and W. Zhang, Photonics Res. **11**(3), 431 (2023).
[46]H. Zhang, X. Zhang, Q. Xu, C. Tian, Q. Wang, Y. Xu, Y. Li, J. Gu, Z. Tian, C. Ouyang, X. Zhang, C. Hu, J. Han, and W. Zhang, Adv. Opt. Mater. **6**(1), 1700773 (2018).
[47]H. Zhang, X. Zhang, Q. Xu, Q. Wang, Y. Xu, M. Wei, Y. Li, J. Gu, Z. Tian, C. Ouyang, X. Zhang, C. Hu, J. Han, and W. Zhang, Photonics Res. **6**(1), 24 (2018).
[48]W. Liu, Q. Yang, Q. Xu, X. Jiang, T. Wu, J. Gu, J. Han, and W. Zhang, Nanophotonics **11**(16), 3631 (2022).
[49]J. Fan and Y. Cheng, J. Phys. D **53**(2), 025109 (2020).
[50]N. K. Grady, J. E. Heyes, D. R. Chowdhury, Y. Zeng, M. T. Reiten, A. K. Azad, A. J. Taylor, D. A. Dalvit, and H. T. Chen, Science **340**(6138), 1304 (2013).
[51]N. Yu, P. Genevet, M. A. Kats, F. Aieta, J. P. Tetienne, F. Capasso, and Z. Gaburro, Science **334**(6054), 333 (2011).
[52]S. Walia, C. M. Shah, P. Gutruf, H. Nili, D. Chowdhury, W. Withayachumnankul, M. Bhaskaran, and S. Sriram, Appl. Phys. Rev. **2**(1), 011303 (2015).
[53]Q. Wang, X. Zhang, E. Plum, Q. Xu, M. Wei, Y. Xu, H. Zhang, Y. Liao, J. Gu, J. Han, and W. Zhang, Adv. Opt. Mater. **5**(14), 1700277 (2017).
[54]Y. V. Grachev, A. Gorodetsky, N. S. Balbekin, M. S. Kulya, B. Sokolenko, and N. V. Petrov, Proc. SPIE **11906**, 119061N (2021).
[55]A. K. Kaveev, G. I. Kropotov, E. V. Tsygankova, I. A. Tzibizov, S. D. Ganichev, S. N. Danilov, P. Olbrich, C. Zoth, E. G. Kaveeva, A. I. Zhdanov, A. A. Ivanov, R. Z. Deyanov, and B. Redlich, Appl. Opt. **52**(4), B60 (2013).
[56]N. V. Petrov, B. Sokolenko, M. S. Kulya, A. Gorodetsky, and A. V. Chernykh, Light: Adv. Manuf. **3**(4), 44 (2022).
[57]V. V. Kotlyar, A. A. Kovalev, and A. P. Porfirev, Opt. Express **27**(8), 11236 (2019).
[58]I. A. Litvin, A. Dudley, and A. Forbes, Opt. Express **19**(18), 16760 (2011).
[59]X. Ding, F. Monticone, K. Zhang, L. Zhang, D. Gao, S. N. Burokur, A. de Lustrac, Q. Wu, C. W. Qiu, and A. Alu, Adv. Mater. **27**(7), 1195 (2015).
[60]F. Monticone, N. M. Estakhri, and A. Alu, Phys. Rev. Lett. **110**(20), 203903 (2013).
[61]Y. Xu, Q. Xu, X. Zhang, X. Feng, Y. Lu, X. Zhang, M. Kang, J. Han, and W. Zhang, Adv. Funct. Mater. **32**(44), 2207269 (2022).